ACS OMEGA

Open Access

http://pubs.acs.org/journal/acsodf

Article

Experimental Study on the Backflow Mechanism of Proppants in Induced Fractures and Fiber Sand Control Under the Condition of Large-Scale and Fully Measurable Flow Field

Yixin Chen,* Yu Sang, Jianchun Guo,* Jian Yang, Weihua Chen, Botao Tang, Feng Feng, Xinghao Gou, and Yifan Zhang

Cite This: *ACS Omega* 2023, 8, 42467−42478

Read Online

ACCESS | Metrics & More | Article Recommendations

ABSTRACT: The proppant backflow in the process of flowback has a great significant effect on gas field development. Therefore, the study of proppant backflow is of great significance for the development and production of gas wells. At present, the physical simulation methods for proppant backflow mainly include the tube perforation model, the slot model, an API standard flow tester, and a large-scale flowback apparatus. The current experimental methods are unable to observe the backflow of proppants during the process of the flowback test. In addition, the only characterization parameter for proppant backflow is the liquid flow rate corresponding to the sand discharge in the diversion chamber called critical velocity, which is too simple and single to accurately characterize the movement state of proppants during the flowback process. In this paper, a physical simulation method of proppant backflow in fractures based on the measurement of flow field was proposed. It can realize the observation and fine description of the proppant backflow state and movement rule. In addition, the process of proppant backflow can be quantitatively described by a multidimensional characterization parameter. The research shows that (1) the proppant backflow is closely related to the shape of the sand bank formed during the proppant placement and the irregular voids formed; (2) the fiber increases the strength of the proppant pack significantly; (3) the critical velocity with fiber increased by 2.25 times compared with the critical velocity without fiber, the optimum fiber concentration was 0.8%, and the fiber length was 12 mm; (4) the full fiber injection was selected as the best injection mode by the experiment; and (5) the whole process of flowback can be divided into two stages. In the strong fluid shear stage, the effect of fiber sand control is more significant. However, when the flowback enters the stage of slow erosion, the difference in the sand control effect under different parameters is no longer significant.

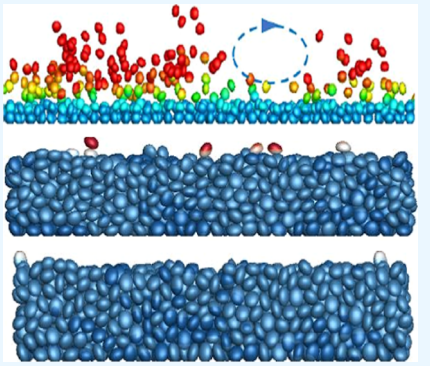

1. INTRODUCTION

Hydraulic fracturing is an important technology in gas field development and widely used in various gas field stimulations. The flowback is an important part of hydraulic fracturing construction, which has an important impact on the overall fracturing effect. According to the current on-site flowback of tight gas wells after fracturing, there is a common phenomenon of proppant backflow. According to incomplete statistics, the proppant backflow rate of tight gas horizontal wells in the JQ block ranges from 3.7 to 15.3%. The backflow of proppants will produce fracture face skin effect,[1,2] forming a fracture damage zone near the wellbore which results in reducing the effective support area of the fracture and its conductivity, thereby affecting the production capacity of the gas well. Related studies have shown that the average gas production decline rate of proppant backflow gas wells is more than 3 times that of normal production wells.[3] In addition, the accumulation of backflow proppants at the bottom of the well buries the gas layer or causes erosion of surface pipelines when it is discharged from the wellhead, and so on, which poses safety hazards in construction and production.[4,5] Therefore, the study of proppant backflow is of great significance for the development and production of gas wells.

The existing physical simulation experimental methods to research proppant backflow mainly include the following: (1) tube perforation model: the experimental device mainly consists of a fluid inlet and an outlet, a sand collector, a circular tube, and a proppant pack[6] (see Figure 1).

The experimental method is to first fill the circular tube with proppants, then saturate the proppant pack with the experimental fluid, and continuously increase the fluid pumping rate until the proppants occur in the sand collector. At this point,

Received: July 13, 2023
Revised: October 7, 2023
Accepted: October 11, 2023
Published: November 1, 2023

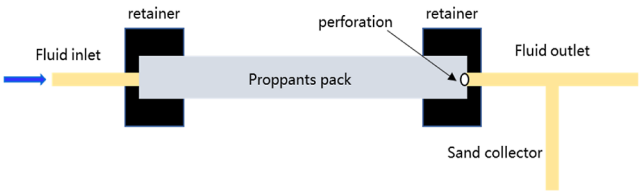

Figure 1. Tube perforation model experimental device diagram.

the corresponding fluid velocity is defined as the critical velocity of proppant backflow, which characterizes the law of proppant backflow.[7]

(2) Slot model: the slot is a parallel plate device which is 17 cm high and 24 cm long with provisions for varying fracture gap width.[8] The slot is filled with proppants to simulate a propped fracture; then, the closure pressure is applied with actuators to simulate confining pressure on the proppant pack. Water is pumped into the slot to simulate the flowback of the fracturing fluid. The water flow rate is varied until the proppant pack destabilizes, and the sand production begins. The sand distribution is observed in the fracture with a vision system[9] (see Figure 2). The law of proppant backflow is characterized by

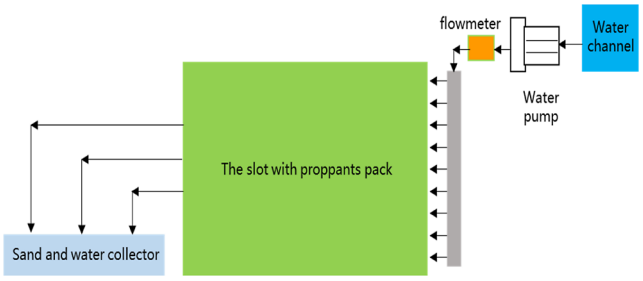

Figure 2. Slot model experimental device diagram.

the fluid velocity which corresponds to the appearance of proppants in the sand collector, defined as the critical velocity of proppant backflow.[10,11]

(3) API standard flow tester: the experimental device is mainly composed of a displacement device, a flowmeter, a diversion chamber, a hydraulic press, etc. The experimental method is to first fill the proppants in the diversion chamber and then apply the closed pressure to the proppant pack through a hydraulic press.[12] The experimental fluid saturates the proppant pack by the displacement device. The experimental fluid velocity is increased step by step, until sand production is observed in the diversion chamber. At this time, the corresponding fluid velocity is defined as the critical velocity of proppant backflow, which characterizes the law of proppant backflow.[13,14]

(4) Large-scale flowback apparatus: the device mainly consists of a flowback cell, a hydraulic press equipped with a heating system water pump, an 8-gal water bath, a set of sensors (thermocouples, flowmeters, and pressure gauge), a data acquisition system, and a computer (see Figure 3). Prior to testing, the flowback cell is water-sealed with a silicone rubber compound and rubber O-rings.[15] To test flowback stability, a proppant pack is sandwiched between two plates. Closure stress is applied normally to the proppant pack, and it is kept constant at the set point for the duration of the test by an electronically controlled syringe pump. Tap water or mixtures of tap water and glycerol (50:50 by volume) are heated up in a dedicated water bath up to the required temperature (usually 104 °F) and pumped through the flowback cell by a water pump with a stepping rate from 0.1 to 5.3 gal/min (with a constant rate increment of 0.2 gal/min and a ramp slope at acceleration of 0.4 gal/min). Pumping pressure and fluid temperature are measured before the inlet face of the proppant pack, which allows monitoring of the test conditions and calculation of the differential pressure. Proppant pack height is measured by a digital depth gauge. The law of proppant backflow characterized by the fluid velocity corresponds to the appearance of proppants in the sand collector, defined as the critical velocity of proppant backflow.

In summary, the existing physical simulation experimental methods for proppant backflow research are all based on filling the diversion chamber with proppants to form a stable and continuous proppant pack, ignoring the influence of the proppant migration process and the shape of the sand bank on proppant backflow. However, in fact, the shape of the sand bank, which is controlled by proppant migration during the actual fracturing process, has a significant impact on the fluidization zone of proppant pack. Second, the current experimental methods are unable to observe the backflow of proppants during the process of flowback test and cannot accurately characterize the state and pattern of proppant backflow. Third, there is a significant difference between the current experimental scale and the actual fracture geometry on site, which reflects a certain gap in the backflow characteristics of the proppants compared to the actual on-site conditions.

In addition, the only characterization parameters for proppant backflow under current experimental methods are the liquid flow rate corresponding to the sand discharge in the diversion chamber, which is the critical velocity of proppant backflow.[16] The characterization parameters are too simple and single to accurately characterize the movement state of proppants during

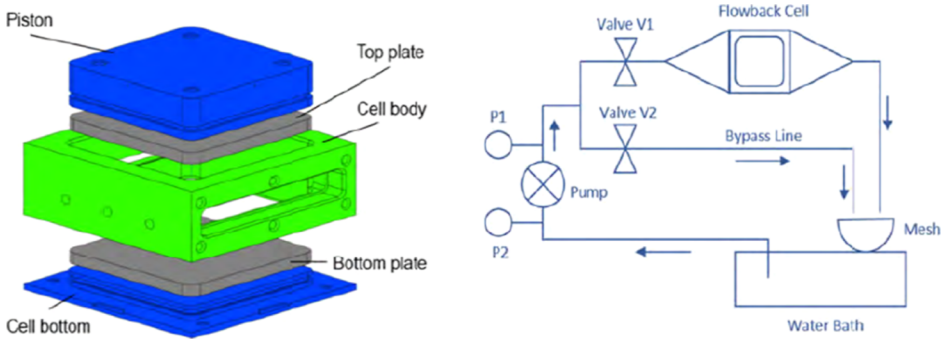

Figure 3. Flowback cell of large-scale flowback apparatus (left) and schematic of flow loop (right).

https://doi.org/10.1021/acsomega.3c05030
ACS Omega 2023, 8, 42467−42478

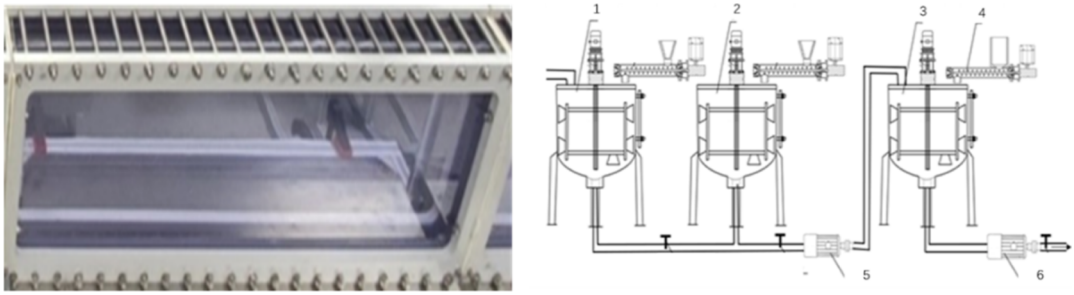

Figure 4. Fracture module of FPM (left) and circulation pump module of FPM (right).

the flowback process (starting, rolling, and settling of proppants) and various parameters during the movement process (fluid velocity, particle velocity, and velocity gradient).[17]

To solve the above problems, a physical simulation method of proppant backflow in fractures based on the measurement of flow field was proposed. This method utilizes a self-developed experimental device. The device consists of four parts: the fractures and circulation pump module (FPM), the laser test module (LTM), the image capture module (ICM), and the data processing module (DPM). The FCPM can simulate the migration and settlement of proppants in fractures during fracturing construction, as well as the initiation and migration of proppants during flowback.[18] Through the LTM, ICM, and DPM in combination with the ion separation algorithm, cross-correlation principle PIV algorithm, and PTV algorithm, it can realize the observation and fine description of the proppant backflow state and movement rule under the condition of considering the shape of the sand bank and proppant placement.[19,20] In addition, the process of proppant backflow can be quantitatively described by multidimensional characterization parameters (such as the shape of the sand bank, the local morphology changes of the sand bank, the flow field of the fracturing fluid, the proppant particle field, longitudinal fluid velocity, and velocity gradient) which are measured by the device. Therefore, the law of proppant backflow can be revealed.

2. METHODOLOGY

2.1. Experimental Device. *2.1.1. Fractures and Circulation Pump Module.* The fracture module consists of two plexiglass plates and an external metal frame. The thickness of the plexiglass plate is less than 3 cm, and its high light transmittance enables the laser to enter the middle of the fracture at a small refraction angle, which does not affect the observation of the fracture interior, and the laser information incident on the flow field can be collected by the shooting system. The size of the fracture module is about 100 × 30 cm, and the simulated fracture in the experiment is composed of four fracture modules. The circulation pump module consists of a mixing unit, a pumping unit, and a circulation unit. The work is completed by using two 300 L liquid mixing tanks (1, 2) with agitators, one 300 L sand mixing tank (3, 4) with agitators, and two G35-2 screw pumps (5, 6), Figure 4.

The fracturing fluid is configured in two mixing tanks and pumped into the sand mixing tank by the liquid supply pump. At the same time, the sand addition device is adjusted to ensure that the proppants are added into the sand mixing tank at a designed rate. After the proppant and fracturing fluid are fully mixed in the sand mixing tank, the sand carrying fluid is pumped into the fracture through the sand carrying pump. The entire experimental process achieved a high degree of similarity to that of the on-site construction process.

2.1.2. Laser Test and ICM. LTM and ICM are key devices for achieving quantitative testing of the migration of fluid and proppants in fracture. It is mainly composed of a laser emitter, an optical regulator, a high-speed camera, a synchronization signal triggering device, and a real-time image processing system.

Its working principle is to convert the point-like laser emitted by the laser emitter into a sheet laser through the optical regulator during the liquid flow field test to light up all surfaces in the flow field. A high-speed camera is used to receive the laser reflected by the tracer particles in the flow field from the front of the simulated fracture so as to obtain the motion image of the tracer particles and transmit it to the computer. Then, the real-time image processing system can be used to analyze the velocity field of the fluid in the test area. In addition, the synchronization signal triggering device ensures coordinated operation between the laser and camera. When the velocity field of proppants in fracture is tested, a light source is injected from one side of the plate, and the light intensity varies after penetrating the gap between proppants in the flow field. On the other side of the plate, a high-speed camera is used to receive the penetrated light and generate an image that is transmitted to a computer. Then, the particle velocity field can be obtained through a real-time image processing system.

The laser emitter mentioned above is a high-performance Nd/Yag double-cavity double-pulse high-power lasers produced by Evergreen Company in the United States. The parameters of the sCMOS high-speed camera selected for a high-speed camera are shown in Table 1. The synchronization signal triggering device selected the Programmed Time Unit produced by Germany LaVision.

Table 1. Parameters of the sCMOS Camera

name	parameters
resolution ratio	2560 × 2160 pixel
photography frequency	1000 Hz
shot	Nikon 50 mm f/1.8
interface method	Camera Link
sensor	CMOS 11 μm^2

2.1.3. Data Processing Module. The core of information discrimination, representation, and velocity interpretation of particle images is pixel level computation. First, the properties of each pixel (exposure value) and the characteristics of each pixel group (exposure area size) were analyzed and calculated to distinguish proppant particles from tracer particles. Then, pixel images representing proppants and tracer particles were respectively targeted. The PIV algorithm was used to calculate

https://doi.org/10.1021/acsomega.3c05030
ACS Omega 2023, 8, 42467−42478

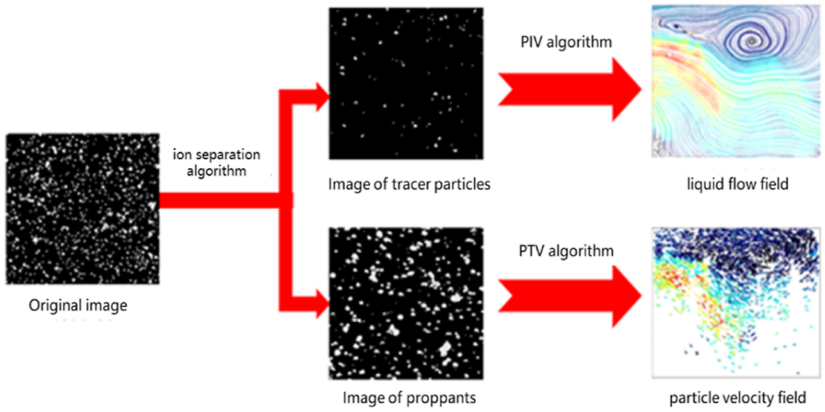

Figure 5. Computational structure of data processing systems.

the pixel coordinates corresponding to the tracer particle pixel image to obtain the fracturing fluid velocity field. The proppant velocity field was obtained by calculating the pixel coordinates corresponding to the proppant pixel image using the PTV algorithm. A set of quantitative characterization algorithm systems including particle separation algorithm, PIV algorithm based on cross-correlation principle, and PTV algorithm was used, and velocity postprocessing characterization was an important supplement. Figure 5 shows the structure of the entire test system. In this paper, image enhancement, particle image separation, proppant velocity calculation, and particle temperature calculation were all implemented by MATLAB programming, and the fracturing fluid flow field velocity was calculated by DAVIS software. Proppant velocity field display was implemented using the ePython programming language.

2.2. Experimental Design. The purpose of this experiment is to study the mechanism of proppant backflow and the effect of fiber on proppant backflow control. The materials and processes used in the experiment are consistent with field fracturing construction. The process of proppant migration involves injecting 70/140 mesh quartz sand, followed by 40/70 mesh-coated sand in an 8:2 ratio of quartz sand to coated sand. The viscosity of the slick water is 30 mPa s in the experiment, which is the same as that of the field construction fluid. The process of sand injection is consistent with the on-site construction, and the sand concentration is increased by steps of 120, 360, and 480 kg/m^3. According to the Reynolds number similarity principle, the field displacement is converted into the displacement of the laboratory sand transport process, which can be queried in Table 2. In the flowback process, the broken liquid with a viscosity of 5 mPa·s will be used for reverse injection, and the corresponding experimental displacement will be queried in Table 2 according to the field flowback situation. Table 3 shows the overall scheme of proppant backflow and fiber sand control experiment.

The parameter characterization in the experiment can be divided into four categories: (1) morphological changes of sand bank before and after flowback.

The morphological change can directly reflect the scour ability of the fluid to the sand bank. In this paper, ICM was used to record the changing process of the sand bank in the four flat devices, and the macro outline of the sand bank was formed through image mosaic so as to analyze the migration characteristics of the proppants in the flowback process under different conditions (see Figure 6).

(2) Height variation of the sand bank. The change in the height of the sand bank during the flowback process can reflect the degree of fluid erosion of the proppant pack. In this paper, a high-speed camera was used to record the variation of height of the sand bank in the area of 197 × 171 mm, and the variation curve of height of the sand bank with time was drawn to find the critical velocity of strong shear affecting the height of the sand bank (see Figure 7).

(3) Fracturing fluid flow field and proppant particle field (see Figure 8). The fracturing fluid flow field and proppant velocity field can be obtained by the Davis program and the Matlab separation algorithm. Matlab can output the position of proppant particles on two frames of images. Through the position information and time difference of particles, parameters such as angle, speed, and quantity of particles can be further extracted. Through the above methods, microscopic motion information of proppants in the flowback process was obtained in this paper to reveal the mechanism of proppant flowback motion.

(4) Longitudinal fluid velocity and velocity gradient (Figure 9). The shear force of the fluid on the surface of the sand dike is related to the velocity gradient. Therefore, Davis software was

Table 2. Corresponding Table of Actual Displacement on Site and Indoor Experimental Flow[a]

H_e, m	W_e, mm	H_f, m	W_f, mm	Q_f, m^3/min	Q_e, L/min
0.3	5	30	10	1	0.25
0.3	5	30	10	2	0.5
0.3	5	30	10	3	0.75
0.3	5	30	10	4	1
0.3	5	30	10	5	1.25
0.3	5	30	10	6	1.5
0.3	5	30	10	7	1.75
0.3	5	30	10	8	2
0.3	5	30	10	9	2.25
0.3	5	30	10	10	2.5
0.3	5	30	10	11	2.75
0.3	5	30	10	12	3
0.3	5	30	10	13	3.25
0.3	5	30	10	14	3.5
0.3	5	30	10	15	3.75
0.3	5	30	10	16	4
0.3	5	30	10	17	4.25
0.3	5	30	10	18	4.5

[a]In Table 2, H_e is the simulated fracture height, W_e is the simulated fracture width, H_f is the actual fracture height, W_f, is the actual fracture width, Q_f, is the actual field displacement, and Q_e is the laboratory displacement.

https://doi.org/10.1021/acsomega.3c05030
ACS Omega 2023, 8, 42467−42478

Table 3. Experimental Plan of Proppant Backflow and Fiber Sand Control

no	concentration of fiber (%)	length of fiber (mm)	injection mode	experimental displacement	factor	materials
1	0	6	full fiber injection	0.3L−5L/min	concentration of fiber	the concentrations of proppants are 120 kg/m^3, 360 kg/m^3, and 480 kg/m^3, respectively; 30 mPa·s slick water for fracturing and 5 mPa·s slick water for flowback; 40/70-coated sand +70/140 quartz sand
2	0.4					
3	0.8					
4	1.2					
5	0.8	3	full fiber injection		length of fiber	
6		12				
7	0.8	6	alternate injection		injection mode	
8			fiber tail injection			
9	0.4	12	full fiber injection		time	
10						
11	1.2					

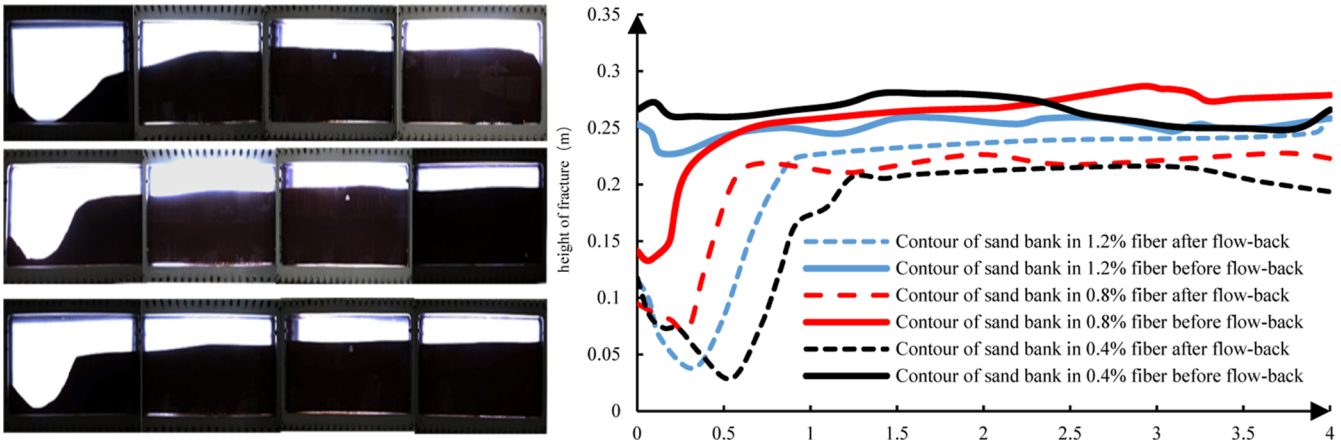

Figure 6. Actual sand bank (left) and extracted sand bank contour (right).

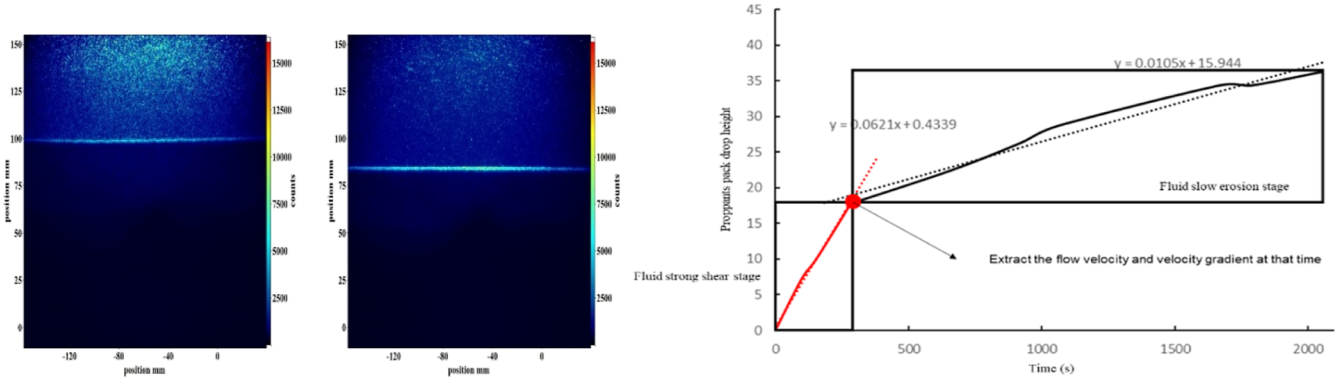

Figure 7. Changes in sand bank height (left) and variation curve of sand bank height with time (right).

used to obtain the horizontal velocity of the fluid in the longitudinal direction and calculate the velocity gradient change, which reflects the shear action of the fluid on the proppant-filled layer to a certain extent.

3. RESULTS AND DISCUSSION

3.1. Effect of Time on Proppant Backflow. From the fiber sand carrying experiment (see Figure 10), it was found that the injection of fibers and the increase in fiber concentration can effectively delay the settling of the proppants, resulting in the proppant pack consisting of a large amount of a fluffy mixture of proppants and fibers. The gaps between these mixtures will become good channels for fluid flow during the flowback process, which has a certain promoting effect on the backflow of the proppants.

Over time, the proppants settled and eventually reached a stable state, and the spaces between the mixtures gradually compacted. The flowback process of the proppant packed in a

https://doi.org/10.1021/acsomega.3c05030
ACS Omega 2023, 8, 42467−42478

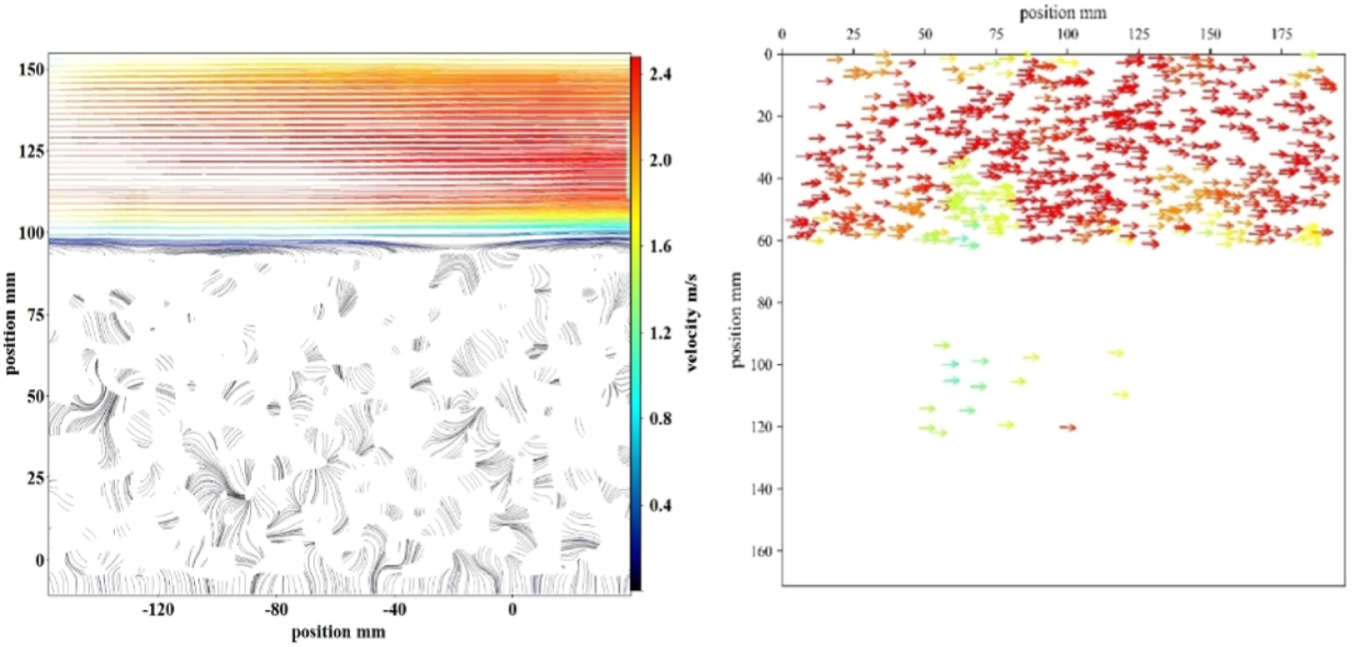

Figure 8. Fracturing fluid flow field (left) and proppant particle field (right).

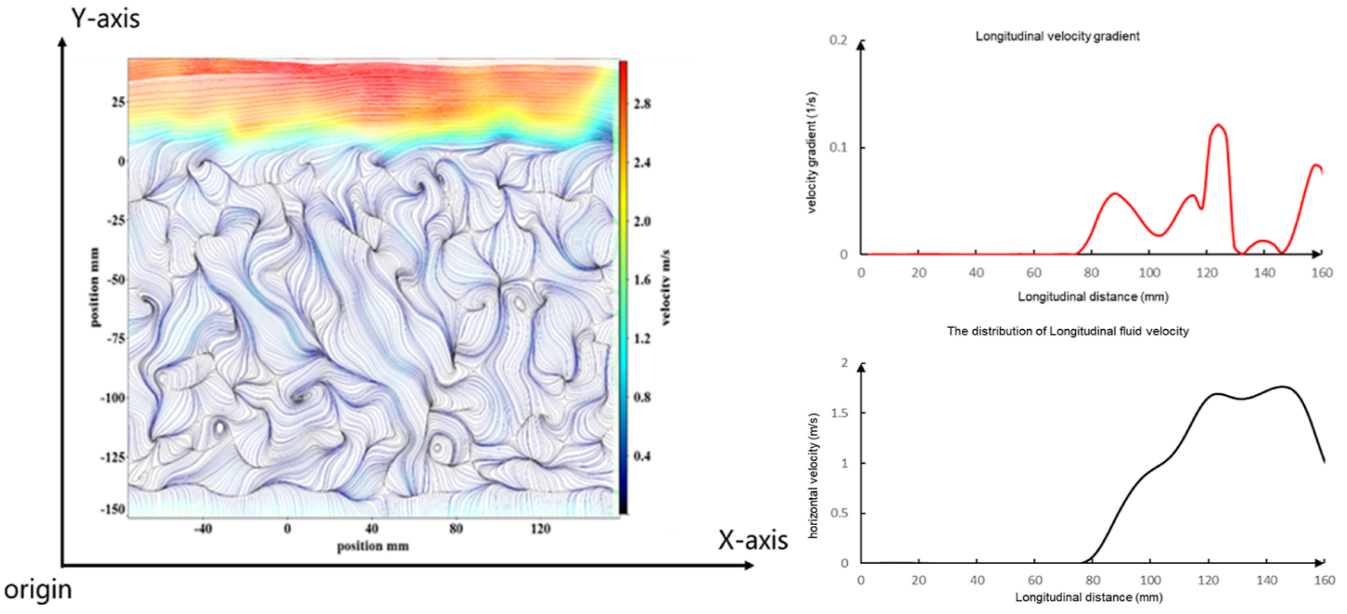

Figure 9. Longitudinal fluid velocity and velocity gradient.

Figure 10. Proppant pack consisting of a fluffy fiber−proppant mixture in a fiber sand carrying experiment.

steady state is closer to the actual situation in the field. The experimental results indicate that the proppant pack can fully reach a stable state after being left standing for 12 h after the end of the pump injection. Therefore, the subsequent proppant backflow law research experiments will be conducted after completing the pump injection for 12 h.

3.2. Effect of Different Fiber Concentration on Proppant Backflow. According to the experimental plan in Table 3, the fiber concentrations are 0, 0.4, 0.8, and 1.2%. The following figures show the morphologies of different sand banks in different experimental stages.

Figure 11 shows that as the fiber concentration increases, the proppants settled more slowly and were transported farther,

https://doi.org/10.1021/acsomega.3c05030
ACS Omega 2023, 8, 42467−42478

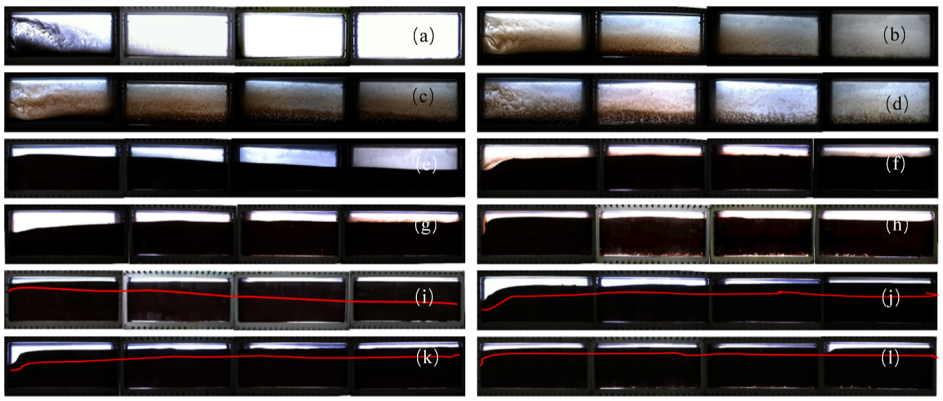

Figure 11. Shape of the sand bank at different experimental stages: (a−d) proppant placement during the early pumping process with different fiber concentrations (0, 0.4, 0.8, and 1.2%, respectively); (e−h) shape of the sand bank before trailing the coated sand with different fiber concentrations; and (i−l) shape of the sand bank after trailing the coated sand with different fiber concentrations.

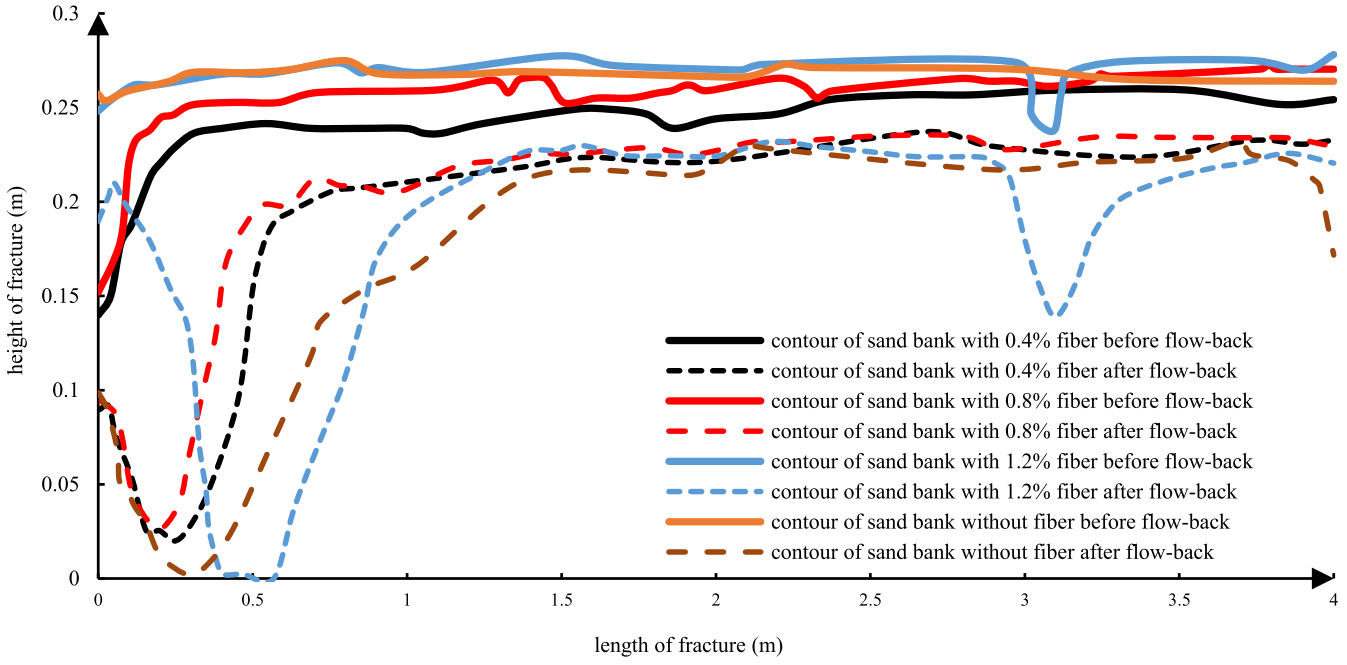

Figure 12. Contour of the sand bank before and after flowback with different fiber concentrations. (a) In the strong fluid shear stage, the sand bank has a sharp undulation pattern, and the amount of proppants is washed up; (b) in the stage of slow erosion, a small number of proppants on the surface of the sand bank were washed away by the fluid, and the proppant backflow in a rolling manner; and (c) when the flow rate is lower than the critical velocity, the proppants bite each other and no longer backflow.

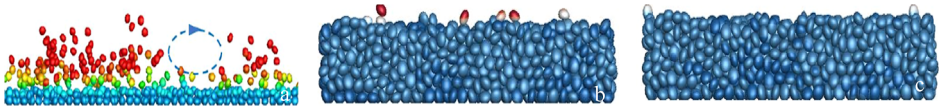

Figure 13. Proppant movement mode in different stages of flowback. (a) Change of the descending height of the sand bank with time under the condition of 0.4% fiber concentration during flowback; (b) change of the descending height of the sand bank with time under the condition of 0.8% fiber concentration during flowback; and (c) change of the descending height of the sand bank with time under the condition of 1.2% fiber concentration during flowback.

resulting in a higher sand bank and larger intergranular pores in the proppant pack. In addition, it shows that the proppant pack formed at the end of pumping becomes looser as the amount of fiber is added. In addition, the trailing-coated sand is carried by a large amount of fluid to the upper part of the sand bank or carried to the far end of the fracture, failing to form effective sealing at the end of the fracture, Figure 12.

To effectively evaluate the distribution pattern of the sand bank during the flowback, the channel rate (CR) of the fracture is introduced

$$\mathrm{CR} = \frac{S_u}{S_p} \tag{1}$$

CR is the CR of the fracture, %; S_u is the area without proppants in the fracture, m^2; and S_p is the whole area of the fracture.

https://doi.org/10.1021/acsomega.3c05030
ACS Omega 2023, 8, 42467−42478

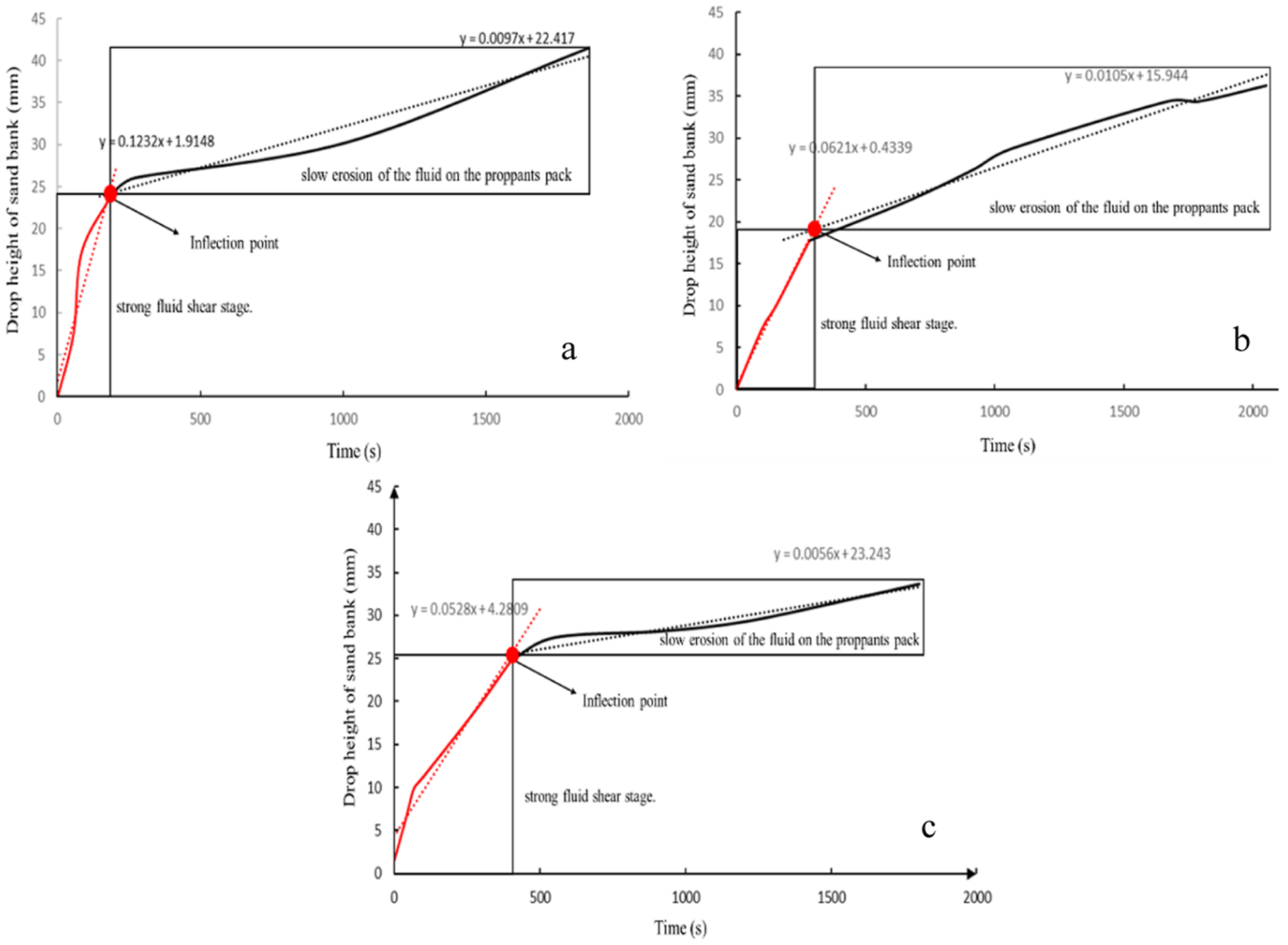

Figure 14. Relationship between the descending height of the sand bank and time under different fiber concentrations. (a) Flow field and particle field in the stage of strong fluid shear and (b) flow field and particle field in the stage of slow erosion of the fluid on the proppant pack.

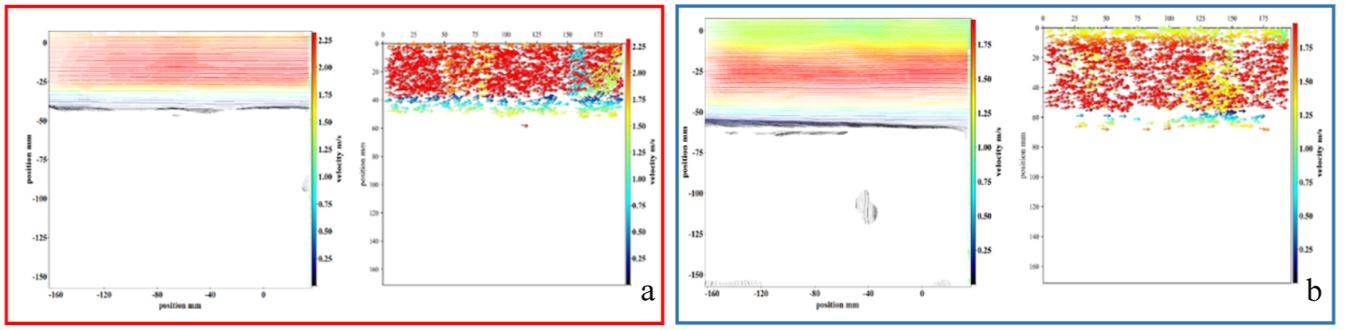

Figure 15. Microscopic flow field and particle field during flowback.

Through the CR calculation, it is found that when the fiber dosage is 0, 0.4, 0.8, and 1.2%, the corresponding CRs are 0.47, 0.38, 0.34, and 0.3, respectively. It is initially recognized that the fiber can effectively reduce proppant backflow during the flowback process, and the blocking effect becomes more obvious with the increase of fiber concentration.

Figure 13 shows the local morphology changes of the sand bank before and after flowback. The experimental results show that proppant backflow mainly occurs at the top of the proppant pack. It is mainly manifested as the erosion of proppant caused by the strong shear action caused by the high-speed flow of fluid. This process is mainly divided into two stages. At the beginning of flowback, due to the small space at the top of the proppant pack, the fluid flows so fast that causes a strong erosion on the proppant pack, resulting in a large number of proppant backflow. During the experiment, it shows a rapid decrease in the height of the sand bank. This is called the strong fluid shear stage. As time goes on, the loss of proppants increases the area of the fluid flow channel, gradually slows down the fluid flow rate, and leads to a gradual decrease in the degree of erosion of the proppant pack. During the experiment, it shows that the height of the sand bank drops slowly. This stage is the slow erosion of the fluid on the proppant pack.

https://doi.org/10.1021/acsomega.3c05030
ACS Omega 2023, 8, 42467−42478

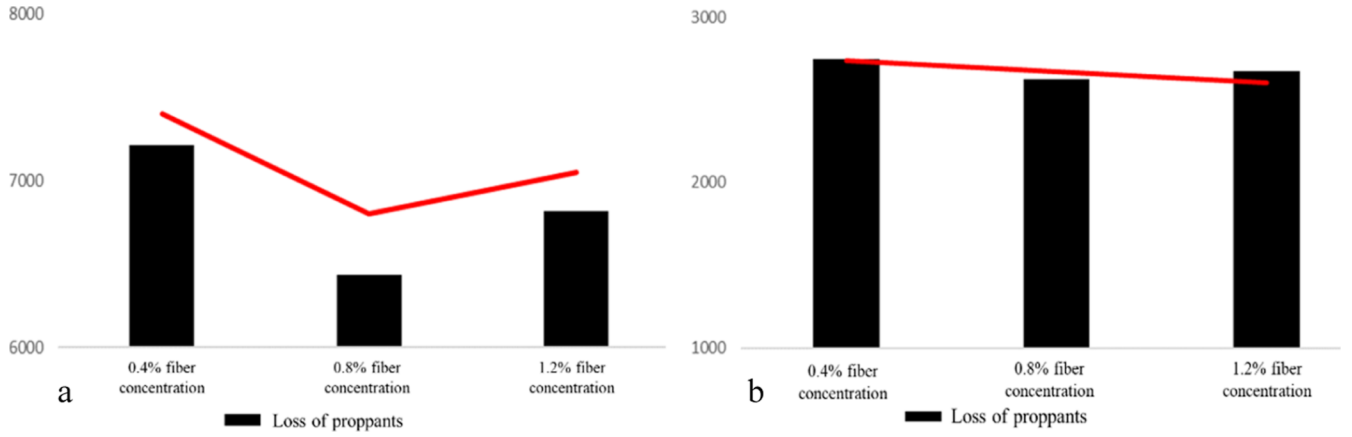

Figure 16. Loss of proppants under different fiber concentrations in two stages. (a) Stage of strong fluid shear and (b) stage of slow erosion of the fluid on the proppant pack.

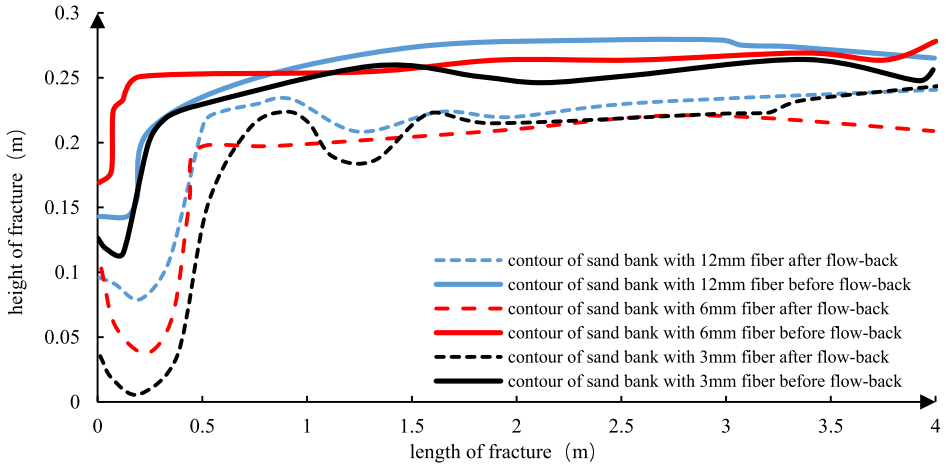

Figure 17. Contour of the sand bank before and after flowback with different fiber lengths. (a) Change of the descending height of the sand bank with time under the condition of 3 mm fiber length; (b) change of the descending height of the sand bank with time under the condition of 6 mm fiber length; and (c) change of the descending height of the sand bank with time under the condition of 12 mm fiber length.

These two stages can also be well reflected in the relationship curve between the descending height of the sand bank and time (Figure 14). In the curve, there is a clear inflection point between the two stages. The earlier the inflection point appears, the more severe the proppant pack is eroded by the fluid. The large amount of proppant loss causes the channel of the fluid flow to become larger, allowing the flowback to enter the slow fluid erosion stage earlier. (This view can be confirmed in the microscopic flow field and particle field, as shown in Figure 15.) The later the inflection point occurs, the longer the strong fluid shear stage lasts, indicating that the proppant pack is more resistant to fluid erosion. The experimental results show that with the increase of fiber concentration, the inflection point appears later, which shows that the fiber concentration plays a significant role in improving the strength of the proppant pack and resisting fluid erosion.

The velocity at the inflection point (called critical velocity) is extracted, and the characteristics of the flow field at the inflection point are further analyzed by PIV. It was found that under the conditions of 0, 0.4, 0.8, and 1.2% concentration of fiber, the critical velocities are 1.03 1.89, 2.26, and 2.32 m/s, respectively, which further confirms that the ability of the proppant pack to resist fluid erosion increased with the increase of fiber addition. By extracting the loss of proppants in two stages, it was found that during the stage of strong fluid shear, the fiber concentration has a significant resistance to fluid erosion in the proppant pack (see Figure 16a). However, in the stage of slow erosion of the fluid on the proppant pack, the effect of fiber concentration on the resistance of the proppant pack to fluid erosion is no longer significant (see Figure 16b).

3.3. Effect of Different Fiber Lengths on Proppant Backflow. Figure 17 shows the shape of the sand bank before and after flowback with different fiber lengths. The calculated CRs under different fiber lengths (3, 6, and 12 mm) are 0.38, 0.34, and 0.29, respectively, which indicate that the proppant pack becomes more resistant to fluid action with the increase of fiber length.

Figure 18 shows that the stage of strong fluid shear lasted longer with the increase of fiber length, which indicates that the longer the fiber, the more resistant the proppant pack to fluid erosion. Extracting the velocity field of the inflection point can calculate the critical velocity of 1.94, 2.12, and 2.26 m/s for different fiber lengths.

By extracting the loss of proppants in two stages, it was found that during the stage of strong fluid shear, the fiber length has a significant resistance to fluid erosion in the proppant pack (see Figure 19a). However, in the stage of slow erosion of the fluid on the proppant pack, the effect of fiber length on the resistance of

https://doi.org/10.1021/acsomega.3c05030
ACS Omega 2023, 8, 42467−42478

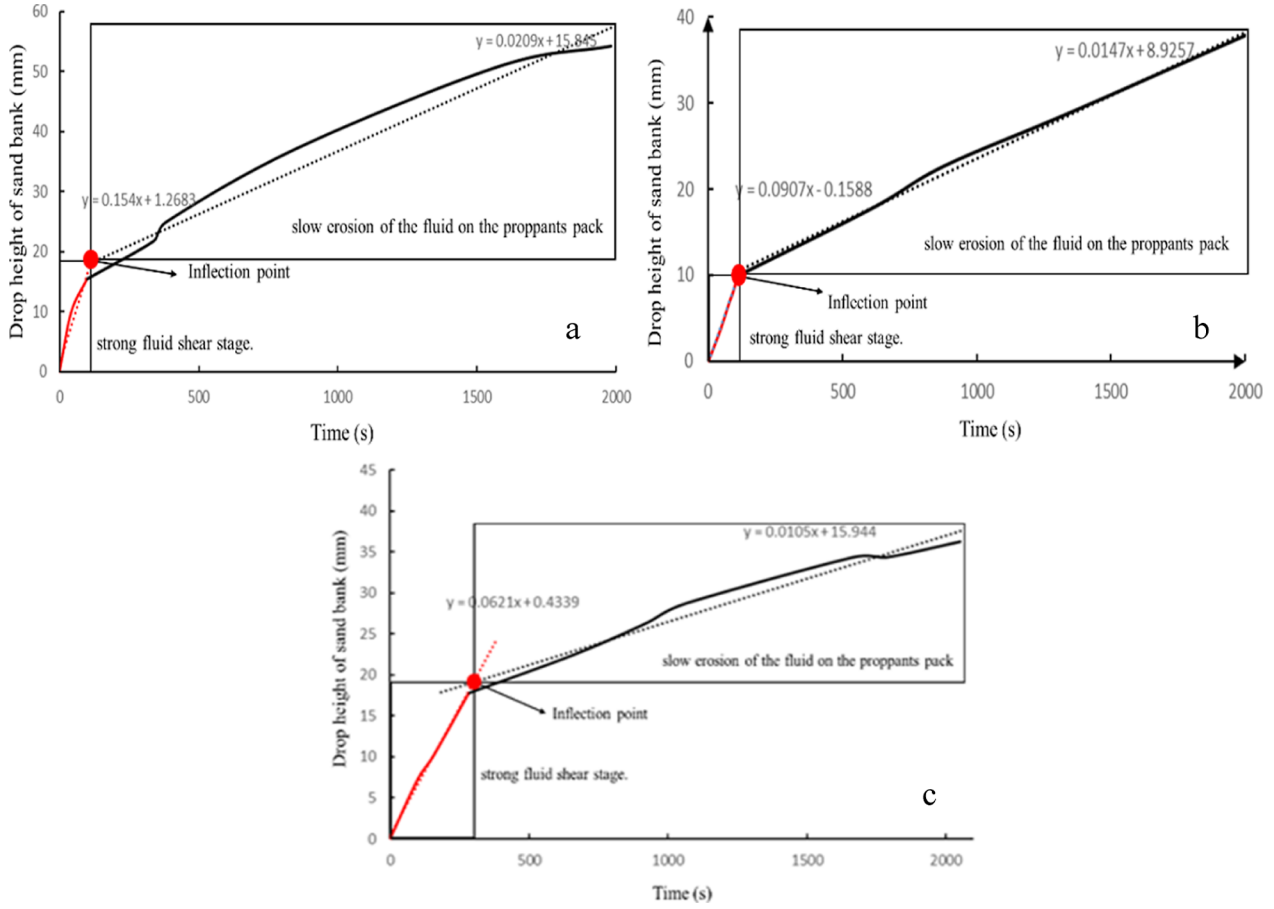

Figure 18. Relationship between the descending height of the sand bank and time under different fiber lengths.

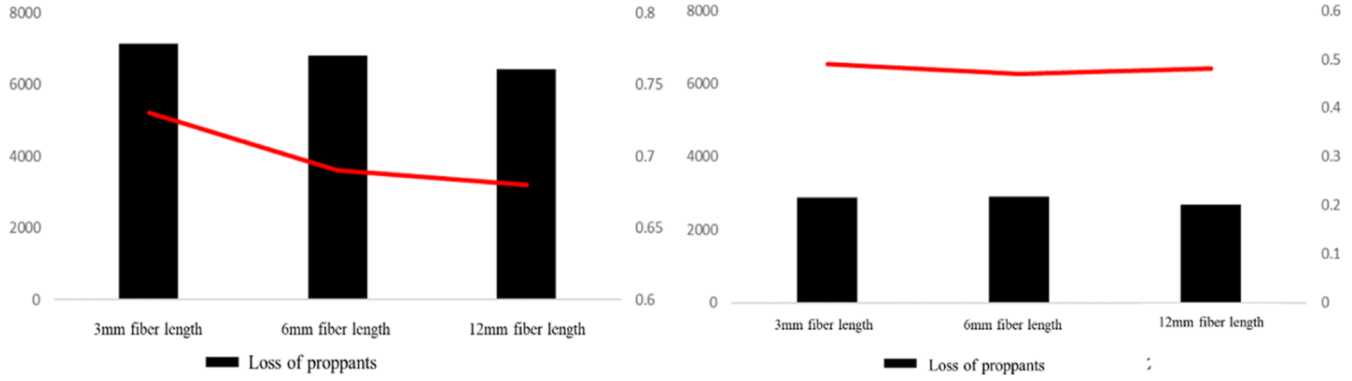

Figure 19. Loss of proppants under different fiber lengths in two stages: (a) stage of strong fluid shear and (b) stage of slow erosion of the fluid on the proppant pack.

the proppant pack to fluid erosion is no longer significant (see Figure 19b).

3.4. Influence of Different Injection Modes on Proppant Backflow. Figure 20 shows the shape of the sand bank before and after flowback with different fiber injection modes. The calculated CRs under different fiber injection modes are 0.43, 0.42, and 0.34, respectively. It is obvious to observe that the full fiber injection is the most significant increase in the strength of the proppant pack to resist the fluid erosion. In addition, the proppant pack formed by other injection modes is less resistant to fluid erosion.

According to the curve of relationship between the descending height of sand bank and time, the time to reach the slow erosion stage in the flowback process under different injection modes is 60, 85, and 244 s, respectively, and the critical velocities are 1.87, 2.06, and 2.24 m/s, respectively. The experimental results show that the fibers are effective in preventing proppant backflow.

4. CONCLUSIONS

The following understandings are obtained through experiments.

(1) In previous studies, it was believed that the stability of the hemispherical sand arch formed by the proppants in the perforation area is the key to affecting the proppant backflow. However, this experiment found that the

https://doi.org/10.1021/acsomega.3c05030
ACS Omega 2023, 8, 42467−42478

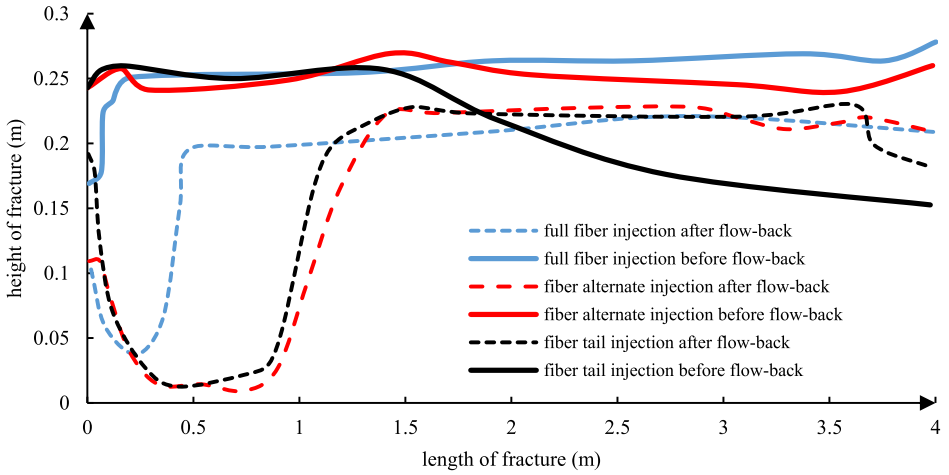

Figure 20. Contour of the sand bank before and after flowback with different fiber injection modes.

proppant backflow is closely related to the shape of the sand bank formed during the proppant placement and the irregular voids formed. From the experimental results, it can be seen that the process based on end of the fracture sealing to prevent proppant backflow has certain limitations. The results of this experiment indicate that the trailing coated sand is carried by a large amount of fluid to the upper part of the sand bank or carried to the far end of the fracture, failing to form effective sealing at the end of the fracture.

(2) The whole process of flowback can be divided into two stages. At the beginning of flowback, due to the small space at the top of the proppant pack, the fluid flows so fast that causes a strong erosion on the proppant pack, resulting in a large number of proppant backflow. In this stage, the sand bank has a sharp undulation pattern, and amounts of proppants are washed up. As time goes on, the loss of proppants increases the area of the fluid flow channel, gradually slows down the fluid flow rate, and leads to a gradual decrease in the degree of erosion of the proppant pack. In this stage, a small number of proppants on the surface of the sand bank were washed away by the fluid and the proppant backflow in a rolling manner. When the flow rate is lower than the critical velocity, the proppants bite each other and no longer backflow. In addition, in the strong fluid shear stage, the effect of fiber sand control is more significant. However, when the flowback enters the stage of slow erosion, the difference in sand control effect under different parameters is no longer significant.

(3) The fiber increases the strength of the proppant pack significantly, and the addition of the fiber makes the proppant pack more resistant to flowback fluid erosion. The critical velocity with fiber increased by 2.25 times compared with the critical velocity without fiber. The experimental results show that the critical flow rate increases with the increase of fiber concentration and length. The optimum fiber concentration was 0.8%, and the fiber length was 12 mm. In addition, the full fiber injection was selected as the best injection mode by the experiment.

(4) In view of the limitations of the existing proppant backflow simulation experiments, such as small fracture scale, simple and single characterization parameters, and rough characterization of backflow motion patterns, a physical simulation method of proppant backflow in fractures based on the measurement of flow field was proposed, which achieves precise characterization of proppant backflow motion patterns under large-scale conditions. At the same time, the backflow process of proppants is quantitatively described through multi-dimensional characterization parameters.

AUTHOR INFORMATION

Corresponding Authors

Yixin Chen − *PetroChina Southwest Oil and Gas Field Company, Chengdu, Sichuan 646002, China*; orcid.org/0000-0003-0234-9583; Email: 494358688@qq.com

Jianchun Guo − *Southwest Petroleum University, Chengdu, Sichuan 610500, China*; Email: guojianchun@vip.163.com

Authors

Yu Sang − *PetroChina Southwest Oil and Gas Field Company, Chengdu, Sichuan 646002, China*

Jian Yang − *PetroChina Southwest Oil and Gas Field Company, Chengdu, Sichuan 646002, China*

Weihua Chen − *PetroChina Southwest Oil and Gas Field Company, Chengdu, Sichuan 646002, China*

Botao Tang − *PetroChina Southwest Oil and Gas Field Company, Chengdu, Sichuan 646002, China*

Feng Feng − *PetroChina Southwest Oil and Gas Field Company, Chengdu, Sichuan 646002, China*

Xinghao Gou − *PetroChina Southwest Oil and Gas Field Company, Chengdu, Sichuan 646002, China*

Yifan Zhang − *Southwest Petroleum University, Chengdu, Sichuan 610500, China*

Complete contact information is available at: https://pubs.acs.org/10.1021/acsomega.3c05030

Notes

The authors declare no competing financial interest.

ACKNOWLEDGMENTS

The authors would like to acknowledge the financial support of the key projects supported by the joint fund of the National Natural Science Foundation of China (U21A20105) and the research project of proppant flowback mechanism and fiber-based proppant flowback control technique in the process of

https://doi.org/10.1021/acsomega.3c05030
ACS Omega 2023, 8, 42467−42478

flowback after fracturing in a horizontal well in Shaximiao formation tight gas reservoir of Petro-China Southwest Oil & Gas field Company (20220302-24).

REFERENCES

(1) Goel, N. Experimental Investigation of Proppant Flow-back Phenomena Using a Large-Scale Fracturing Simulator[C]. *SPE Annual Technical Conference and Exhibition*; SPE, 1999.
(2) Canon, J. Avoiding Proppant Flow-back in Tight-Gas Completions with Improved Fracture Design[C]. *SPE Annual Technical Conference and Exhibition*; SPE, 2003.
(3) Dimitry, C. Proppant Flow-back: Can We Mitigate the Risk? [C]. *SPE Hydraulic Fracturing Technology Conference and Exhibition held in The Woodlands*; SPE: Texas, USA, 2020.
(4) Ramlan, A.; Zin, R.; Abu Bakar, N. F.; Othman, N. H. Recent progress on proppant laboratory testing method: Characterisation, conductivity, transportation, and erosivity. *J. Petrol. Sci. Eng.* **2021**, *205*, 108871.
(5) Barree, R.; Miskimins, J.; Conway, M. et al. *Generic Correlations for Proppant Pack Conductivity. Paperpresented at the SPE Hydraulic Fracturing Technology Conference*; The Woodlands: Texas, USA, 2016; pp 9−11 February.SPE-179135-MS.
(6) Canon, J.; Romero, D.; Pham, T.; et al. Avoiding Proppant Flowback in Tight-Gas Completions withImproved Fracture Design. *Paper presented at the SPE Technical Conference and Exhibition*; SPE: Denver, CO, 2003; pp 5−8 October. SPE-84310-MS.
(7) Garagash, I.; Osiptsov, A.; Boronin, S. Dynamic Bridging of Proppant Particles in a Hydraulic Fracture. *Int. J. Eng. Sci.* **2019**, *135*, 86−101.
(8) Guo, B.; Ugwu, D. An Experimental Investigation of the Critical Flow-back Velocity in Hydraulic-Fracturing Shale Gas Wells. *Hydraul. Fract. J.* **2015**, *2* (1), 19−25.
(9) McLennan, J.; Walton, I.; Moore, J.; Brinton, D.; Lund, J. Proppant Backflow: Mechanical and Flow Considerations. *Geothermics* **2015**, *57*, 224−237.
(10) Ismail, N. I.; Kuang, S.; Yu, A. CFD-DEM study of particle-fluid flow and retention performance of sand screen. *Powder Technol.* **2021**, *378* (378), 410−420.
(11) Horadam, W.; Venkat, N.; Tran, T.; Bai, L.; Josyula, K.; Mehta, V. Leaching studies on Novolacresin-coated proppants-performance, stability, product safety, and environmental health considerations[J]. *J. Appl. Polym. Sci.* **2018**, *135*, 45845.
(12) Zhang, Z.; Guo, B. The Critical Flow Back Velocity in Hydraulic-Fracturing Shale Gas Wells. *Int. J. Publ. Probl. Appl. Eng. Res.* **2016**, *6* (2), 7−11.
(13) Peng, Y.; Li, Y. M.; Zhao, J. Z. "A novel approach to simulate the stress and displacement fields induced by hydraulic fractures under arbitrarily distributed inner pressure,". *J. Nat. Gas Sci. Eng.* **2016**, *35* (35), 1079−1087.
(14) Serdyuk, A.; Frolenkov, A.; Valeev, S.; et al. Multistage Stimulation of Sidetrack Wellbores Utilizing Fiber-Enhanced Plugs Proves Efficient for Brown Oil Fields Development. *Paper presented at the International Petroleum Technology Conference*; IPTC: Bangkok, Thailand, 2016; pp 14−16 November. IPTC-18987-MS.
(15) Zhou, X.; Ma, Y.; Liu, M.; et al. New measurements on hydrodynamics in a gas-liquid-solid expanded bed. *J. Particuology* **2021**, *58* (16), 276−284.
(16) Cheng, K.; Zhu, J.; Qian, F., et al. CFD-DEM simulation of particle deposition characteristics of pleated air filter media based on porous media model[J]. **2022**.
(17) Benedito, W.; Duarte, C.; Barrozo, M.; et al. Cataracting-centrifuging transition investigation using non-spherical and spherical particles in a rotary drum through CFD simulations. *J. Particuology* **2022**, *60* (1), 48.
(18) He, L.; Liu, Z.; Zhao, Y. An extended unresolved CFD-DEM coupling method for simulation of fluid and non-spherical particles. *J. Particuology* **2022**, *68* (9), 1.
(19) Wu, Y.; Liu, D.; Hu, J.; Ma, J.; Chen, X. Comparative study of two fluid model and dense discrete phase model for simulations of gas−solid hydrodynamics in circulating fluidized beds. *Particuology* **2021**, *55*, 108−117.
(20) Lei, H.; Zhu, L.; Luo, Z. Study of fluid cell coarsening for CFD-DEM simulations of poly-disperse gas-solid flows. *J. Particuology* **2023**, *73* (2), 128.

https://doi.org/10.1021/acsomega.3c05030
ACS Omega 2023, 8, 42467−42478